Electric polarisation switching in an atomically-thin binary rock salt structure

Jose Martinez-Castro[1,2,3,†], Marten Piantek[3,4], Sonja Schubert[3,5], Mats Persson[6,7], David Serrate[3,4,5*], and Cyrus F. Hirjibehedin[1,2,8**]

[1]London Centre for Nanotechnology, University College London (UCL), London WC1H 0AH, UK.
[2]Department of Physics & Astronomy, UCL, London WC1E 6BT, UK.
[3]Instituto de Nanociencia de Aragón and Laboratorio de Microscopías Avanzadas, Universidad de Zaragoza, 50018 Zaragoza, Spain
[4]Fundación Instituto de Nanociencia de Aragón (FINA), 50018, Zaragoza, Spain
[5]Departamento de Física de la Materia Condensada, Universidad de Zaragoza, 50009 Zaragoza, Spain
[6]Surface Science Research Centre and Department of Chemistry, University of Liverpool, Liverpool, L69 3BX, UK
[7]Department of Physics, Chalmers University of Technology, SE-412 96, Göteborg, Sweden
[8]Department of Chemistry, UCL, London WC1H 0AJ, UK.
[†]present address: Department of Quantum Matter Physics, University of Geneva, 1211 Geneva 4, Switzerland.
[*]email: serrate@unizar.es
[**]email: c.hirjibehedin@ucl.ac.uk

Published in *Nature Nanotechnology* (2017)

Inducing and controlling electric dipoles is hindered in the ultrathin limit by the finite screening length of surface charges at metal-insulator junctions [1-3], though this effect can be circumvented by specially designed interfaces [4]. Heterostructures of insulating materials hold great promise, as confirmed by perovskite oxide superlattices with compositional substitution used to artificially break the structural inversion symmetry [5,6,7,8]. Bringing this concept to the ultrathin limit would substantially broaden the range of materials and functionalities that could be exploited in novel nanoscale device designs. Here, we report that non-zero electric polarisation can be induced and reversed in a hysteretic manner in bilayers made of ultrathin insulators whose electric polarisation cannot be switched individually. In particular, we explore the interface between ionic rock salt alkali halides such as NaCl or KBr and polar insulating Cu_2N terminating bulk copper. The strong compositional asymmetry between the polar Cu_2N and the vacuum gap breaks inversion symmetry in the alkali halide layer, inducing out of plane dipoles that are stabilised in one orientation (self-poling). The dipole orientation can be reversed by a critical electric field, producing sharp switching of the tunnel current passing through the junction.

Provided that the total thickness of the insulating stack allows electron tunnelling, an ideal tool to access the electrostatic properties of ultrathin insulating layers is scanning tunnelling microscopy (STM) in combination with atomic force microscopy (AFM). These techniques have been applied to investigate the electronic properties of metal oxides [9,10] and nitrides [11,12], binary rock salts such as NaCl [13], and ultrathin ferroelectrics on graphene [14]. In addition, the STM setup introduces a device-like geometry where the vacuum gap between tip and sample avoids the need for a top electrode and breaks sharply the inversion symmetry at the Cu_2N-NaCl interface.

As seen in Fig. 1, STM (see Supplementary Methods) can be used to confirm that NaCl forms atomically thin layers when deposited on Cu_2N/Cu(001). With atomically resolved STM imaging and from a comparison to prior STM and density functional theory (DFT) calculations of NaCl [15] and Cu_2N/Cu(001) [16], it is possible to determine the binding geometry of NaCl layers on Cu_2N/Cu(001). Figure 1b shows that, at large negative bias voltages, bright spots corresponding to Cl atoms in the NaCl monolayer appear on top of hollow sites of Cu_2N, while dark spots corresponding to Na atoms appear on top of N atoms (see illustration in

Supplementary Fig. 1). For the NaCl bilayer, bright spots of the bilayer appear on top of the dark sites of the monolayer and vice versa, suggesting the regular NaCl stacking order is preserved in these ultra-thin layers.

Since ultra-thin layers of NaCl are ionic insulators [13] and Cu_2N on Cu(001) [12] is polar and insulating, one needs to consider their electrostatic interactions. From DFT calculations (see Supplementary Methods), the electrostatic potential is found to be positive above both the Cu and hollow sites and negative above the N sites on Cu_2N (Supplementary Fig. 2a). Placing the Cl anions on top of the Hollow site (i.e. surrounded by four Cu atoms) and the Na cations on top of the N should therefore result in the most energetically favourable configuration. DFT calculations confirm that this is the minimum energy configuration (Supplementary Table 1 and Supplementary Discussion).

In addition, the DFT calculations suggest that there is negligible electronic rearrangement between the NaCl and Cu_2N (Supplementary Fig. 2b). Furthermore, the calculated partial density of states of Cl *p* and Na *s* states show evidence of very weak interaction with the Cu states, while there is a significant hybridisation of the electronic states for NaCl bilayer on a bare Cu(001) surface (Supplementary Fig. 3).

As seen in Fig. 1b, the NaCl lattice is pseudomorphic to the Cu_2N lattice. DFT calculations not only confirm the epitaxial growth of NaCl over Cu_2N but the vertical relaxations are consistent with the breaking of inversion symmetry on the NaCl layer (Fig. 1c), with Cu_2N on one side of the NaCl bilayer and vacuum on the other. A combination of the 7% biaxial compressive strain (Supplementary Fig. 1) and the dipolar atomic arrangement on Cu_2N/Cu(001), where N atoms are above Cu atoms, induces a rumpling of the NaCl film. Furthermore, the large asymmetry arising from the absence of a top electrode produces self-poling of the polarisation [5] in the NaCl to stabilise one preferred dipole orientation (Fig. 1c). This is in contrast to perovskites oxides with spontaneous polarisation sandwiched between identical electrodes, where both polarisations are equally probable.

The role of Cu_2N in this heterostructure is therefore twofold: it decouples electronically the NaCl from the Cu electrode, and it breaks the NaCl inversion symmetry. Thus, it is interesting to explore the impact of large electric fields on the system. Because of the STM configuration, the moderate voltages applied over sub-nanometre distances correspond to large electric fields (typically of order 1-10 GV/m). To vary the electric field in a controlled manner and remove sensitivity to variations in local density of states at different energies, we change the tip height (Δz) starting at a fixed position z_0 (as determined by the initial setpoint voltage V_{set} and current I_{set}) and record the tunnel current I for several applied (sample) bias voltages V. As has been observed on bare Cu(001) and Cu_2N/Cu(001) [17], our $I(\Delta z)$ measurements at a fixed bias follow the expected exponential behaviour for NaCl bilayer on Cu(001) and NaCl monolayer on Cu_2N/Cu(001) at both positive bias (electric field pointing from sample to tip) and negative bias (electric field pointing from tip to sample), and for NaCl bilayer on Cu_2N/Cu(001) at negative bias.

In stark contrast, as seen in Fig. 2a, a sharp step in $I(\Delta z)$ is observed for the NaCl bilayer on Cu_2N/Cu(001) at positive bias. Here, two different states can be distinguished: one at larger Δz (lower electric field) and another at smaller Δz (higher electric field). The two states are separated by a sharp change in I that occurs when the tip crosses a critical distance Δz_c. In addition, as seen in the inset of Fig. 2a, the change in current near the transition is different depending on whether Δz is increased or decreased (i.e. there is some hysteresis).

For a constant z_0, Δz_c increases linearly as V increases (Fig. 2b), suggesting that this phenomenon is induced by a critical electric field strength E_C [18]. Fitting the points to a linear trend yields E_C of the order of 10 GV/m; this remains relatively constant over a specific NaCl bilayer on Cu_2N region, but can vary by up to 50% for different tips and different surface regions. We estimate that the tip is approximately 3 Å above the outer NaCl layer at regular scanning conditions (V_{set}=-1.3 V, I_{set}=50 pA), making it possible to approach the surface without using high currents that may cause damage, as long as the applied potential difference lies inside the Cu_2N gap [17].

This two-state switching behaviour is also observed in a potassium bromide bilayer deposited on top of Cu_2N/Cu(001). Although the KBr bilayer on Cu_2N/Cu(001) heterostructure (Supplementary Fig. 4) is more complex because of differences in the intralayer vs. interlayer interactions, as manifested in the observed Moirée pattern in the topographic STM imaging, $I(\Delta z)$ measurements show similar switching for sufficiently large positive applied bias voltage and no switching for negative bias. This indicates the observed switching is a general behaviour in heterostructures composed of a binary rock salt above a polar surface, such as an atomically thin ionic insulator on a metal.

In a simple 1D model for tunnelling, the decay rate of the tunnelling current is fixed by the tunnelling barrier height, which in turn is related to the surface dipole moment through the work function [19]. Hence, we interpret the sharp change in current as arising from a modification of the positions of the ions of the rock salt bilayer; this is further supported by the abrupt change in the measured decay length (Fig. 2c-e and Supplementary Fig. 4b) between the two states, which is consistent with a change in polarisation. The sharp change in current can thus be understood in terms of tunnelling electroresistance TER [20,21,22], where the tunnelling barrier is modified when the polarisation in the rock salt layer is abruptly reversed. Since methods used to characterise polarisation switching, as observed for example in bulk ferroelectric materials, are difficult to extend down to nanoscale dimensions, STM-based TER is an ideal method for exploring polarisation switching in atomically thin nanostructures. Furthermore, as seen in Supplementary Figs. 4 and 5, the relative change in current across the step stays constant as a function of V, as would be expected for a switching of the decay length in the barrier between two well-defined values. Similar discontinuities occur for measurements where z is kept constant while changing V. This further substantiates that the polarisation reversal is purely driven by the external applied electric field.

Corresponding measurements of the electrostatic forces were performed by means of AFM (Supplementary Methods). Figure 3a and Supplementary Fig. 4c show the characteristic parabolic variation expected in Kelvin probe measurements of the shift in the resonance frequency Δf of the oscillating AFM cantilever with voltage [23]. As with the tunnel current, a transition in Δf occurs at a critical bias, observed as a dramatic change in Δf at a threshold voltage that again has a linear relationship with tip height. Since Δf is proportional to the gradient of the force between the tip and the surface [23], the sharp change in Δf is indicative of a sudden change in the electrostatic force between the rock salt bilayer and the tip, consistent with a change in the orientation of the rock salt layer polarisation. The linear shift of applied bias voltage at which the transition occurs versus tip retraction distance is in agreement with $I(\Delta z)$ measurements, indicating that this is the same observed phenomenon (Fig. 3b). Since the AFM sensor oscillates over the range of a complete switching cycle (c.f. inset of Fig. 2a), the hysteresis loop cannot be resolved directly in $\Delta f(V)$ measurements for NaCl because each value results from the average of multiple cycles at the phase lock loop; in contrast, a clear and large hysteresis loop is observed for KBr. In both cases, an abrupt increase in the energy dissipated by the cantilever (Fig. 3c) is a clear indicator of a hysteretic process [24] for which each cycle

contributes additively to the dissipated work when switching between different polarisation states.

As seen in Fig. 4a, DFT calculations indicate that the heights of the Na and Cl ions in the top NaCl layer vary significantly in the presence of an electric field; the different Moirée structures of the KBr/Cu_2N/Cu(001) system (Supplementary Fig. 4a) makes performing similar DFT calculations beyond the scope of this work. In NaCl, the rumpling is reversed for fields larger than approximately 5 GV/m, with the Na cations shifting to a higher height than the Cl anions. At a fixed location above the NaCl bilayer, the calculated integrated local density of states (LDOS), which is proportional to I, also increases significantly for electric fields above 9 GV/m (Fig. 4b). This supports the interpretation that the sharp jump in I and Δf as the electric field is increased by changing either Δz or V arises from dipole reversal in the NaCl layers, resulting in the modification of tunnelling barrier (Fig. 4c,d) as well as a concomitant change in the tip-sample electrostatic force. We note that these calculations correspond to an infinitely wide layer of NaCl bilayer on Cu_2N/Cu(001) subjected to a uniform applied electric field. The fact that calculations neglect finite size effects such as island size or inhomogeneity of the substrate may explain why they show a continuous change in both the position of the ions as well as the integrated LDOS while our experiments show a sharp transition. Computationally demanding calculations with large but finite sized (approximately 5 nm × 5 nm) NaCl/Cu_2N islands on bulk Cu(001) under an applied electric field may shed further light on this issue.

It is interesting to note that upon reversal of the applied electric field, both I and Δf return to their original states almost immediately for NaCl, meaning that relatively small hysteresis is observed. Because of the strong self-poling arising from the asymmetry of the interfaces above and below the NaCl (i.e. the Cu_2N and the vacuum gap), it is sensible to assume that only one of the two dipole orientations is stabilised in the absence of the critical electric field at the temperatures at which our studies are performed. Therefore, we do not observe strong bistability for a defect-free NaCl bilayer, in which both states can be easily stabilised under a given set of conditions. However, strong hysteresis is observed, as shown in Supplementary Fig. 6, when the NaCl bilayer is locally modified by inducing atomic defects (Cl^- vacancies), revealing a way to stabilise the high field state. Such stability could be further enhanced by creating more complex structures of vacancies, which has already been demonstrated for Cl vacancies in NaCl [25]. Similar behaviour has been reported for Sr vacancies in ultrathin $SrTiO_3$, which are found to stabilize ferroelectricity [26]. In the same way, placing a third material above the ultra-thin rock salt layer might cause the same hysteresis enhancement [5].

The vacancy-stabilized configuration on NaCl also offers the possibility to examine the spatial extension of the reversed polarisation state. Remarkably, as seen in Supplementary Fig. 7, the switched state can extend across multiple small Cu_2N island, indicating a relatively long range phenomenon that can cross the Cu_2N island boundaries. Future investigation of the spatial dependence, in other pristine materials with larger hysteresis or in the presence of vacancies, may help to elucidate more details on the nature of the switched state.

In summary, we have demonstrated the possibility to induce and switch the polarisation in atomically thin layers of a normally non-polar compound (NaCl and KBr) when placed on another atomically thin polar insulator (Cu_2N) above a metallic electrode. Atomically thin insulators like Cu_2N also allow the polarised layer to be in close proximity to an electrode, which is necessary for many device designs. While a scanning probe tip was used to produce the critical electric field required to induce polarisation switching, the extended nature of the induced switching suggests that a similar result can be induced with a fixed electrode, as would be found in traditional device designs. The observed change in the surface electrostatic

potential makes this system a potentially interesting substrate for the study of other 2D materials such as MoS_2 [27], providing a new way to induce electrostatic gating and measure its influence without the need for external contact electrodes.

References

[1] Junquera, J. & Ghosez, P. Critical thickness for ferroelectricity in perovskite ultrathin films. *Nature* **422**, 605-509 (2003).
[2] Kim, D. J. *et al.* Polarization Relaxation Induced by a Depolarization Field in Ultrathin Ferroelectric BaTiO3 Capacitors. *Phys. Rev. Lett.* **95**, 237602 (2005).
[3] Stengel, M. *et al.* Origin of the dielectric dead layer in nanoscale capacitors. *Nature* **443**, 679-682 (2006).
[4] Stengel, M. *et al.* Enhancement of ferroelectricity at metal-oxide interfaces. *Nat. Mater.* **8**, 392-397 (2009).
[5] Sai, N. *et al.* Compositional Inversion Symmetry Breaking in Ferroelectric Perovskites. *Phys. Rev. Lett.* **84**, 5636-5639 (2000).
[6] Rogdakis, K. *et al.* Tunable ferroelectricity in artificial tri-layer superlattices comprised of non-ferroic components. *Nature Commun.* **3**, 1064 (2012).
[7] Warusawithana, M. P. Artificial Dielectric Superlattices with Broken Inversion Symmetry. *Phys. Rev. Lett.* **90**, 036802 (2003).
[8] Lee, H. N. *et al.* Strong polarization enhancement in asymmetric three-component ferroelectric superlattices. *Nature*. **433**, 395-399 (2005).
[9] Nilius, M., Wallis, T. M. & Ho, W. Influence of a Heterogeneous Al_2O_3 Surface on the Electronic Properties of Single Pd Atoms. *Phys. Rev. Lett.* **90**, 046808 (2003).
[10] Rau, I. G. *et al.* Reaching the Magnetic Anisotropy Limit of a 3d Metal Atom. *Science* **344**, 988-992 (2014).
[11] Leibsle, F. M., Dhesi, S. S., Barrett, S. D. & Robinson, A. W. STM observations of Cu(100)−c(2×2)N surfaces: evidence for attractive interactions and an incommensurate c(2×2) structure. *Surf. Sci.* **317**, 309-320 (1994).
[12] Hirjibehedin, C. F. *et al.* Large Magnetic Anisotropy of a Single Atomic Spin Embedded in a Surface Molecular Network. *Science* **317**, 1199-1203 (2007).
[13] Repp, J., Meyer, G., Olsson, F. E. & Persson, M. Controlling the charge state of individual gold adatoms. *Science* **305**, 493-495 (2004).
[14] Chang, K. *et al.* Discovery of robust in-plane ferroelectricity in atomic thick SnTe. *Science* **353**, 274-278 (2016).
[15] Hebenstreit, W. *et al.* Atomic resolution by STM on ultra-thin films of alkali halides: experiment and local density calculations. *Surf. Sci.* **424**, L321-L328 (1999).
[16] Choi, T., Ruggiero, C. D. & Gupta, J. A. Incommensurability and atomic structure of c(2×2)N/Cu(100): A scanning tunneling microscopy study. *Phys. Rev. B* **78**, 035430 (2008).
[17] Ruggiero, C. D., Choi, T. & Gupta, J. A. Tunneling spectroscopy of ultrathin insulating films: CuN on Cu(100). *Appl. Phys. Lett.* **91**, 253106 (2007).
[18] Qiu, X. H., Nazin, G. V. & Ho, W. Mechanisms of Reversible Conformational Transitions in a Single Molecule. *Phys. Rev. Lett.* **93**, 196806 (2004).
[19] Leung, T. C. *et al.* Relationship between surface dipole, work function and charge transfer: Some exceptions to an established rule. *Phys. Rev. B* **68**, 195408 (2003).
[20] Gajek, M. et al. Tunnel junctions with multiferroic barriers. *Nat. Mater.* **6**, 296-302 (2007).
[21] Garcia, V. *et al.* Giant tunnel electroresistane for non-destructive readout of ferroelectric states. *Nature* **460**, 81-84 (2009).
[22] Kohlstedt, H. *et al.* Theoretical current-voltage characteristics of ferroelectric tunnel junctions. *Phys. Rev. B* **72**, 125341 (2005)
[23] Giessibl, F. J. Advances in atomic force microscopy. *Rev. Mod. Phys.* **75**, 949-983 (2003).

[24] de la Torre, B. Atomic-Scale Variations of the Mechanical Response of 2D Materials Detected by Noncontact Atomic Force Microscopy. *Phys. Rev. Lett.* **116**, 245502 (2016).
[25] Schuler, B. *et al.* Effect of electron-phonon interaction on the formation of one-dimensional electronic states in coupled Cl vacancies. *Phys. Rev. B* **91**, 235443 (2015).
[26] Lee, D. *et al.* Emergence of room-temperature ferroelectricity at reduced dimensions. *Science* **349**, 1314-1317 (2015).
[27] Costanzo, D. *et al.* Gate-Induced superconductivity in atomically thin MoS_2 crystals. *Nat. Nanotechnol*. **16**, 339-344 (2016).

Data availability

Data that support the findings of this paper will be made available online at figshare (DOI: 10.6084/m9.figshare.c.3877858). Additional information can be obtained by contacting the authors.

Acknowledgements

We acknowledge Pavlo Zubko for stimulating discussions. J.M.C. and C.F.H. acknowledge financial support from Specs GmbH and EPSRC [EP/H002367/1]; D.S. and M. Piantek acknowledge funding from MINECO [MAT2013-46593-C6-3-P] and the use of SAI-Universidad de Zaragoza; M. Persson acknowledges computer time allocated on ARCHER through the Materials Chemistry Consortium funded by the EPSRC grant [EP/L000202], on Polaris through N8 HPC funded by the EPSRC grant [EP/K000225/1] and on Chadwick at University of Liverpool.

Author contributions

J.M.C., D.S., and C.F.H. conceived of the project; J.M.C., M. Piantek, S.S. and D.S. performed the experiments and analysed the results; M. Persson performed the DFT calculations; all authors discussed the results and contributed to the writing of the paper.

Additional information

Supplementary information is available in the online version of the paper. Reprints and permissions information is available online at www.nature.com/reprints. Correspondence and requests for materials should be addressed to D.S. and C.F.H.

Competing financial interests

The authors declare no competing financial interests.

Figure Captions

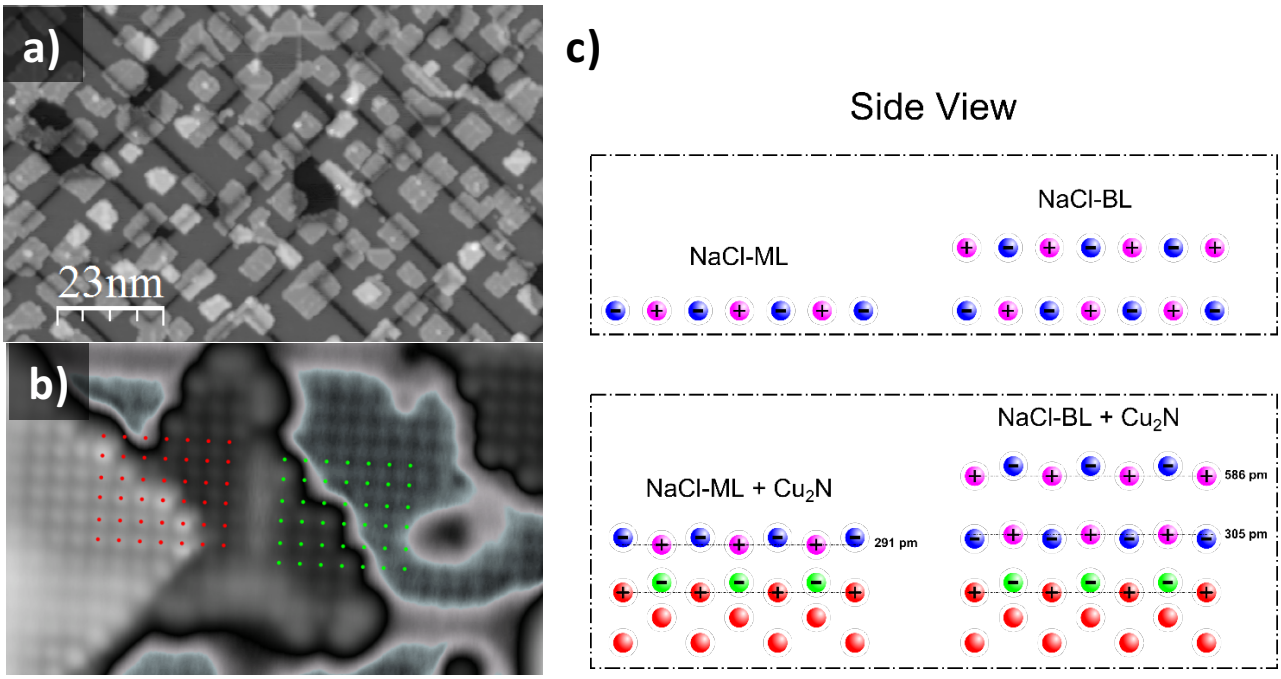

Figure 1 – Ultra-thin NaCl layers on Cu_2N/Cu(001). a) Topographic STM image of a Cu(001) surface fully covered by Cu_2N with monolayers and bilayers of NaCl deposited on top. (72 nm × 116 nm; V_{set}=-1.3 V, I_{set}=50 pA) b) Topographic STM image of a Cu(001) surface mostly covered by Cu_2N islands with small stripes of Cu in between and NaCl monolayer and bilayer on top. Green and red dots indicate the locations of Cl atoms (bright spots) in the NaCl monolayer and bilayer, respectively. (9.5 nm × 9.5 nm; V_{set}=-1.3 V, I_{set}=50 pA) c) Upper illustration shows a side view of Na (purple) and Cl (blue) atoms in an isolated NaCl monolayer and bilayer, as well as a DFT calculation of the structure when it is deposited on a Cu_2N layer containing Cu (red) and N (green) atoms on top of bulk Cu(001). Vertical distance from each NaCl layer to the outermost Cu plane is indicated. Vertical displacements within a layer have been enhanced by a factor of three for visibility.

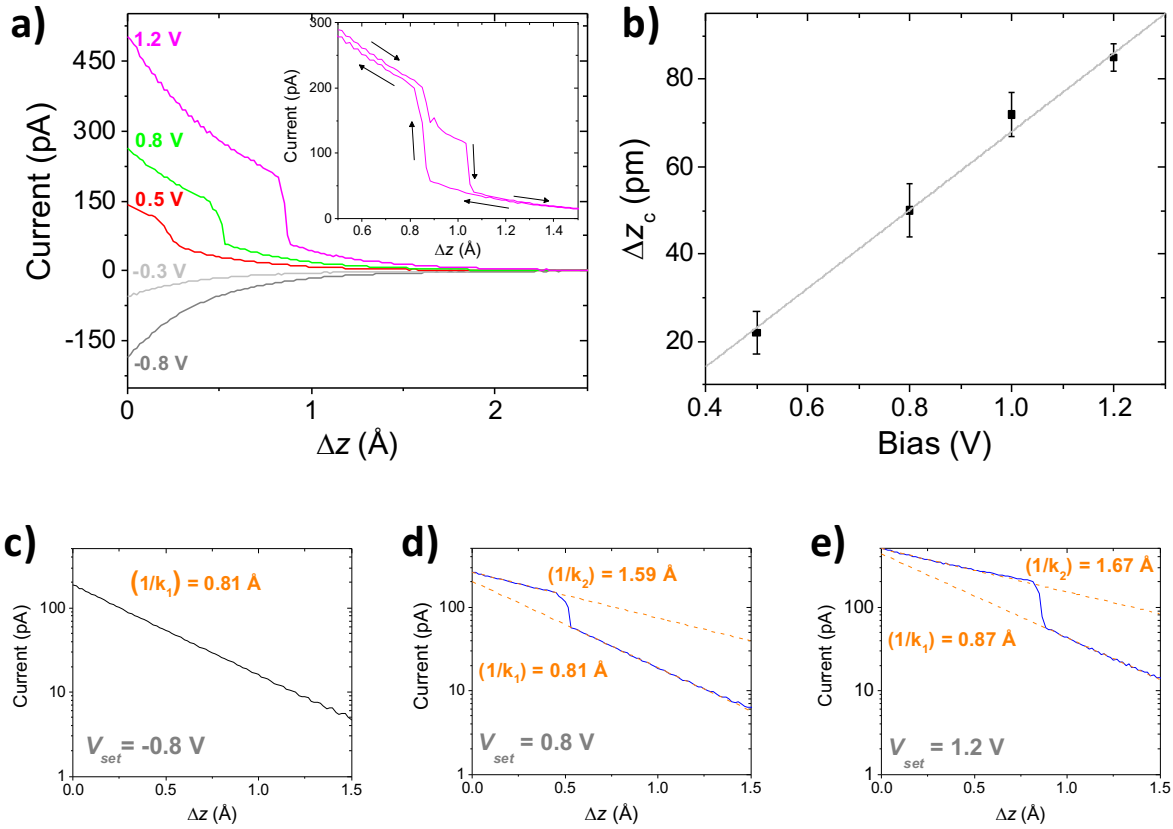

Figure 2 – Electric-field induced switching and calculated decay rates of NaCl bilayer on Cu_2N/Cu(001). a) I vs Δz acquired above the NaCl bilayer on Cu_2N/Cu(001) (V_{set}=-0.8 V, I_{set}=200 pA) for increasing Δz. A clear step in $I(\Delta z)$ is observed for V>0, but not for V<0. The inset shows $I(\Delta z)$ for both increasing and decreasing Δz at V=+1.2 V; weak hysteretic behaviour is observed. b) Change in the Δz_c vs. V, with a best-fit line corresponding to E_c=0.9 GV/m. Vertical error bars represent the width of the step in $I(\Delta z)$. c) $I(\Delta z)$ decay corresponding to the state below the critical electric field shown on a semi-log scale (V_{set} = -0.8 V. The decay length $1/k_{1(2)}$ for state 1(2) is calculated by fitting the current with a simple exponential decay. d) Same as panel c with V_{set} = 0.8 V. A transition between two states is now observed, each with a different current decay length. e) Same as panel c) with V_{set} = 1.2 V. The value of Δz_c changes while the decay lengths for each of the two states remain approximately constant.

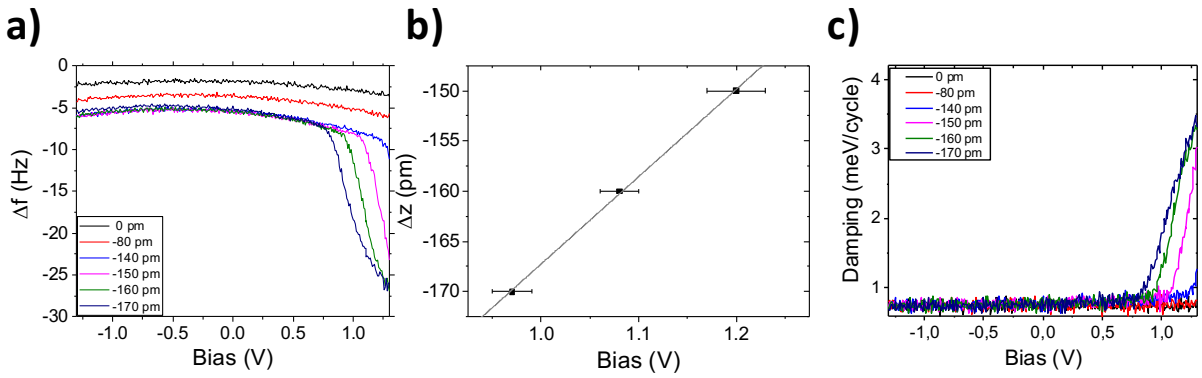

Figure 3 – Force measurements for NaCl bilayer on Cu_2N/Cu(001). $\Delta f(V)$ (Kelvin probe) measurements acquired above the NaCl bilayer on Cu_2N/Cu(001), with a transition in Δf starting at 1.3 V and Δz=-140 pm (V_{set}=-1.3 V, I_{set}=5 pA). b) As expected for an electric field induced effect, the transition shifts linearly towards lower applied bias as the tip-sample distance is decreased**.** The critical transition bias at a given regulation distance is taken from the centre of the transition. Horizontal error bars represent the nearest three measured points from the centre of the transition. c) The increase in dissipation/damping (Supplementary Methods), related to the change in the Kelvin probe parabola, indicates a hysteretic process that is consistent with a ferroelectric cycle.

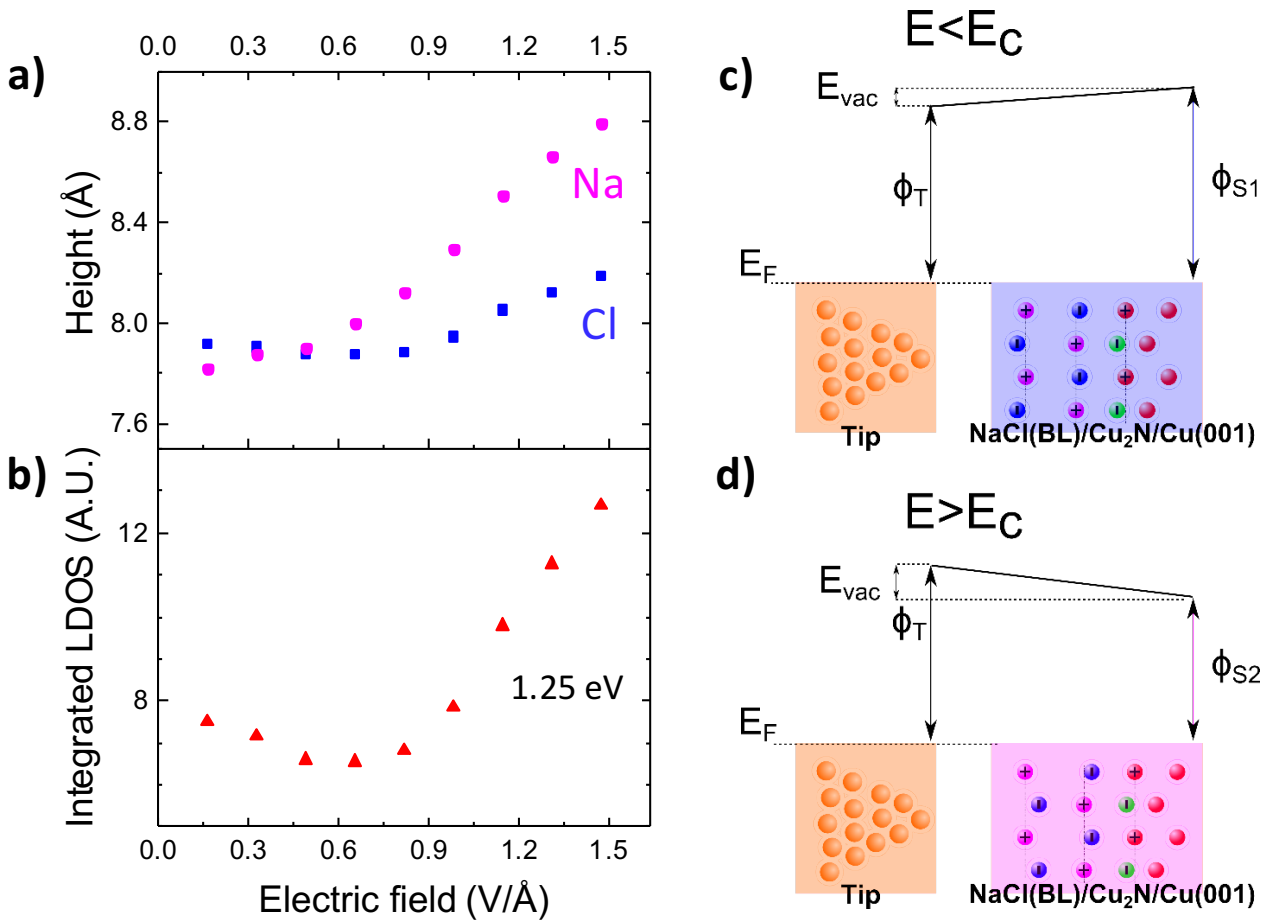

Figure 4 – Electric field induced shift of dipoles in NaCl bilayer on Cu_2N/Cu(001). a) Calculated height, with respect to the bottom layer of Cu atoms in the unit cell, of the topmost Na (magenta) and Cl (blue) atom as a function of applied electric field for NaCl bilayer on Cu_2N/Cu(001) . b) Integrated LDOS from the Fermi level to a sample bias of 1.25 V at a fixed point (2.5 Å above the NaCl surface) as a function of applied electric field. c) Illustration of the positions of Cu (red), N (green), Na (magenta), and Cl (blue) atoms in NaCl bilayer on Cu_2N/Cu(001) for the low electric field configuration from DFT calculations with no electric field. In the outermost layer, the Cl^- atoms sit above the Na^+ atoms, and are thus closer to the tip above. d) Same as panel c for the high electric field configuration from DFT calculations with E=16 GV/m. In the outermost layer, the Cl anions are now below the Na cations, indicating a reversal of the rumpling and therefore also a reversal of the electric dipole.